# DENSE DISCONTINUOUS OPTICAL FLOW VIA CONTOUR-BASED SEGMENTATION

*T. Amiaz and N. Kiryati*

VIA: Vision and Image Analysis Laboratory
School of Electrical Engineering
Tel Aviv University, Tel Aviv 69978, Israel

## ABSTRACT

We propose a new algorithm for dense optical flow computation. Dense optical flow schemes are challenged by the presence of motion discontinuities. In state of the art optical flow methods, over-smoothing of flow discontinuities accounts for most of the error. A breakthrough in the performance of optical flow computation has recently been achieved by Brox *et al*. Our algorithm embeds their functional within a contour-based segmentation framework. Piecewise-smooth flow fields are accommodated and flow boundaries are crisp. Experimental results show the superiority of our algorithm with respect to alternative techniques.

## 1. INTRODUCTION

Optical flow is the apparent motion in an image sequence, observable through intensity variations [1]. Although optical flow is generally not equivalent to the true motion field, they are quite similar in typical cases. Optical flow computation is a key step in many image and video analysis applications, including tracking, surveillance, dynamic super resolution and shape from motion.

Various approaches to optical flow computation have been suggested [2]. These include differential techniques [3, 4], phase based [5] and statistical methods [6]. Variational optical flow computation is a subclass of differential techniques. They use the calculus of variations to minimize a functional embodying the constancy of features in the image and smoothness of the resulting flow. Brox *et al* [7] have significantly improved upon the original work of Horn and Schunck [3], by incorporating coarse-to-fine strategies [8, 9, 10], robust statistics [9, 1] and gradient constancy in a highly nonlinear objective functional.

Dense optical flow methods, i.e. algorithms that estimate the optical flow everywhere in the frame, tend to fail along strong discontinuities in the optical flow field. Even in the algorithm of Brox *et al* [7], that employs a robust smoothness term, most of the error develops there.

This research was supported by MUSCLE: Multimedia Understanding through Semantics, Computation and Learning, a European Network of Excellence funded by the EC 6th Framework IST Programme.

In this paper, we embed the functional of [7] within a contour-based segmentation method. The goal is to profit from the excellent performance of that method, while producing crisp flow boundaries. Inspired by the Mumford-Shah segmentation framework [11], we restate the optical flow problem as that of determining piecewise smooth flow fields bounded by contours, simultaneously minimizing the length of the contours and the optical flow functional of [7] inside the smooth regions.

Due to the presence of unspecified discontinuities in the integration domain, minimization of Mumford-Shah type functionals is difficult. Notable solution approaches include Ambrosio and Tortorelli's $\Gamma$-convergence technique [12], and Vese and Chan's level set method [13]. We follow the latter, because it explicitly limits the width of the boundary.

The proposed objective functional is derived in the next section. The experimental results, presented in section 3, demonstrate tangible performance improvement with respect to the best published methods.

## 2. ALGORITHM

The suggested algorithm combines the superior performance of the algorithm of Brox *et al* [7] in finding smooth optical flow fields, with the ability of Vese and Chan's approach [13] to segment a field into nearly smooth regions.

### 2.1. The optical flow functional of [7]

The optical flow functional represents the following assumptions and constraints:
**Grey level constancy:**

$$I(\vec{x}) = I(\vec{x} + \vec{w}) \tag{1}$$

where $I$ is the image luminance as a function of spatial position and time, and $\vec{w} = (u, v, 1)$ is the optical flow displacement field between the two frames.
**Gradient constancy:** An extension of the grey level constancy assumption, that accommodates illumination changes between the two images.

$$\nabla I(\vec{x}) = \nabla I(\vec{x} + \vec{w}) \tag{2}$$

**Smoothness:** The minimization of a functional relying only on the constancy assumptions is ill posed. A smoothness constraint provides regularization.

**Presence of outliers:** Outliers appear in the flow because of image noise and sharp edges. They are handled in the functional by using robust fidelity and smoothness kernels. Note that in our case segmentation errors will also lead to outliers.

These assumptions lead to the following functional:

$$\begin{aligned} F_{OF}(u,v) &= \int \Psi(|I(\vec{x}+\vec{w})-I(\vec{x})|^2 \\ &\quad +\gamma|\nabla I(\vec{x}+\vec{w})-\nabla I(\vec{x})|^2)d\vec{x} \\ &+ \alpha\int \Psi(|\nabla u|^2+|\nabla v|^2)d\vec{x}\,. \end{aligned} \tag{3}$$

Here $\Psi(x^2)=\sqrt{x^2+\epsilon^2}$ is the modified $L^1$ norm, $\alpha$ is the weight of the smoothness term, and $\gamma$ is the weight of gradient constancy with respect to grey level constancy.

### 2.2. Vese and Chan's segmentation scheme [13]

The level set method [14] is an effective tool for computing evolving contours. It accommodates topological changes and is calculated on a grid. In level set methods, regions are defined by contours that have zero width. This is the motivation for using the level-set segmentation approach in sharpening optical flow discontinuities.

In Vese and Chan's algorithm [13], two smooth fields $u^+$ and $u^-$ approximate the original field and the level-set function $\phi$ indicates the selection between the fields. Defining (local) fidelity

$$f(u)=(u-u_0)^2$$

that compares the field $u$ with the field to be segmented $u_0$, and (local) smoothness

$$s(u)=|\nabla u|^2\,,$$

the following functional is formulated:

$$\begin{aligned} &F_{VC}(u^+,u^-,\phi)= \\ &\quad\int f(u^+)H(\phi)dxdy+\int f(u^-)H(-\phi)dxdy \\ &\quad+\mu\int s(u^+)H(\phi)dxdy+\mu\int s(u^-)H(-\phi)dxdy \\ &\quad+\nu\int|\nabla H(\phi)|dxdy \end{aligned} \tag{4}$$

Here $H(\phi)$ is the Heaviside (step) function of $\phi$. Vese and Chan suggest minimizing this functional by iteratively solving the Euler-Lagrange equations for $u^+$, $u^-$ and $\phi$.

### 2.3. Our piecewise-smooth optical flow functional

Consider again the optical flow functional (3), and identify the expressions of (local) fidelity

$$\begin{aligned} &f(u,v)= \\ &\quad\Psi(|I(\vec{x}+\vec{w})-I(\vec{x})|^2+\gamma|\nabla I(\vec{x}+\vec{w})-\nabla I(\vec{x})|^2) \end{aligned}$$

and (local) smoothness

$$s(u,v)=\Psi(|\nabla u|^2+|\nabla v|^2)\,.$$

The expressions for (local) fidelity and smoothness of the optical flow field are now substituted in the segmentation functional of Vese and Chan (4). Defining the two optical flow fields $\vec{w}^+=(u^+,v^+,1)$ and $\vec{w}^-=(u^-,v^-,1)$, we obtain the proposed objective functional:

$$\begin{aligned} &F(u^+,v^+,u^-,v^-,\phi)= \\ &\quad\int\Psi\left(|I(\vec{x}+\vec{w}^+)-I(\vec{x})|^2\right. \\ &\qquad\left.+\gamma|\nabla I(\vec{x}+\vec{w}^+)-\nabla I(\vec{x})|^2\right)H(\phi)d\vec{x} \\ &\quad+\int\Psi\left(|I(\vec{x}+\vec{w}^-)-I(\vec{x})|^2\right. \\ &\qquad\left.+\gamma|\nabla I(\vec{x}+\vec{w}^-)-\nabla I(\vec{x})|^2\right)H(-\phi)d\vec{x} \\ &\quad+\mu\int\Psi(|\nabla u^+|^2+|\nabla v^+|^2)H(\phi)d\vec{x} \\ &\quad+\mu\int\Psi(|\nabla u^-|^2+|\nabla v^-|^2)H(-\phi)d\vec{x} \\ &\quad+\nu\int|\nabla H(\phi)|d\vec{x} \end{aligned} \tag{5}$$

According to the calculus of variations, a minimizer of this functional must satisfy the Euler-Lagrange equations. The equations for $\vec{w}^+$ and $\vec{w}^-$ are similar to the corresponding equations in [7], but the fidelity (data) term is enabled only where $\phi$ has the proper sign. The smoothness term is left unchanged so it will expand the optical flow field beyond the boundary; this replaces Vese and Chan's method of expanding the field using diffusion. We solve these equations using successive over relaxation.

The Euler-Lagrange equation for $\phi$ is

$$\begin{aligned} \frac{\partial\phi}{\partial t} &= \delta(\phi)\left[\nu\nabla\left(\frac{\nabla\phi}{|\nabla\phi|}\right)-f(u^+,v^+)-\mu s(u^+,v^+)\right. \\ &\quad\left.+f(u^-,v^-)+\mu s(u^-,v^-)\right] \end{aligned} \tag{6}$$

where $\delta(\phi)=H'(\phi)$. We solve this equation using standard discretization of the derivatives and relaxation methods.

Once the solutions $\vec{w}^+,\vec{w}^-$ and $\phi$ are determined, the final estimated optical flow field is:

$$\vec{w}=\begin{cases}\vec{w}^+ & \text{if } \phi>0\\ \vec{w}^- & \text{otherwise}\end{cases} \tag{7}$$

### 2.4. Initialization

The initial values of the fields $\vec{w}^+, \vec{w}^-$ and $\phi$ are obtained by a single application of the original algorithm of [7], followed by a single application of the piecewise-smooth segmentation algorithm of [13]. Following these two steps, the resulting $\phi$ is used for initialization. $\vec{w}^+$ is initialized to

$$\vec{w}^+ = \begin{cases} \vec{w} & \text{if } \phi > 0 \\ \text{avg}_{\phi>0}(\vec{w}) & \text{otherwise} \end{cases} \quad (8)$$

where $\vec{w}$ is the outcome of the first initialization step and $\text{avg}_{\phi>0}(\vec{w})$ is the average of $\vec{w}$ over the region in which $\phi > 0$. The initialization of $\vec{w}^-$ is similar.

## 3. EXPERIMENTAL RESULTS

We present the performance of the algorithm on synthetic and real image sequences. The following parameters (taken from [7, 13]) were used in all the experiments: $\alpha = \mu = 80$, $\gamma = 100$, and the numerical approximation of the Heaviside function $H_\delta(\phi) = \frac{1}{2}(1 + \frac{2}{\pi}\tan^{-1}(\frac{\phi}{\delta}))$ with $\delta = 1$. The number of iterations and $\nu$ were sequence-dependent.

Table 1 compares our algorithm with other dense optical flow algorithms on the *Yosemite* sequence. The angular error was computed as in [2]. The implementation of our algorithm embedded the so-called 2D version of [7], and the performance of our method is compared to that method. Nevertheless, by embedding their 3D version, our method should provide similar improvement with respect to that variant as well. For this sequence, $\nu = 0.02 * 255$ and the number of iterations was 50. Figure 1 shows that the oversmoothing in [7], that forces a gradual change of the optical flow field at the sky-ground interface, is replaced in our method by segmentation of the flow field that is crisp and close ($\leq 2$ pixels) to the ground truth boundaries. The error outside of the sky-ground interface is left unchanged.

Similar performance improvement was achieved on the *Street with car* sequence [15]. The sequence was converted from color to grey-levels. For this sequence, $\nu = 0.05 * 255$ and the number of iterations was 50. Optimal performance of our algorithm, as well as of our implementation of [7], was obtained with Gaussian pre-blurring with $\sigma = 1.0$. The results are presented in Table 2 and in Figure 2.

To test the algorithm on real world data, we used the *Rubic cube* sequence. To demonstrate our algorithm in the presence of optical flow discontinuities, Figure 3 shows the computed flow between the *first* and *last* images in the sequence. It can be seen that the edges of the flow are sharp and that the table is mostly static. For this sequence $\nu = 0.15 * 255$ and the number of iterations was 100.

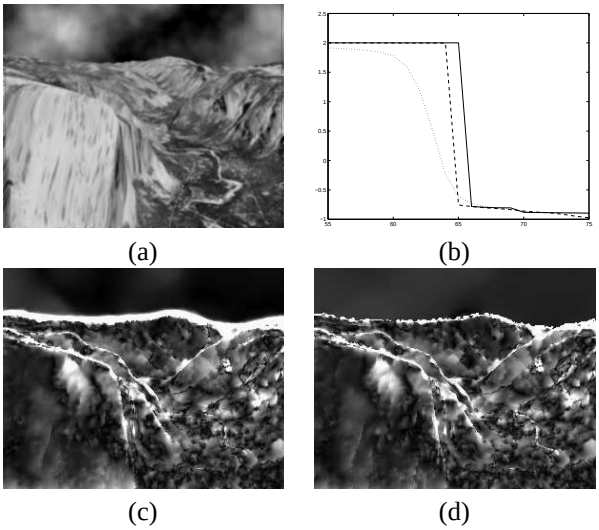

**Fig. 1**. (a) Frame 8 of the *Yosemite* sequence. (b) The horizontal flow as a function of vertical position, at the sky-ground boundary. Solid line: ground truth. Dotted line: Brox *et al*'s 2D result. Dashed line: our result. (c) Angular error in Brox *et al*'s 2D results. Dark means no error. (d) Angular error in our results.

| Technique | AAE | STD |
|---|---|---|
| Horn-Schunck, mod. [2] | 9.78° | 16.19° |
| Mémin-Pérez [10] | 4.69° | 6.89° |
| Brox *et al* (2D) [7] | 2.46° | 7.31° |
| **Our method** | **2.04°** | **7.83°** |

**Table 1**. Comparison between several dense optical flow algorithms on the *Yosemite* sequence. (AAE: Average angular error. STD: Standard deviation of the angular error.)

## 4. CONCLUSION

We presented a novel optical flow algorithm, that embeds Brox *et al*'s optical flow functional within Vese and Chan's segmentation scheme. Performance was boosted by sharpening discontinuities in the optical flow field. Excellent results were shown for image sequences with two dominant motions. Future research should embed optical flow algorithms within Vese and Chan's *four-phase* formulation, thus accommodating more than two dominant motions in the flow field. Better initialization schemes should also be considered, especially for rotational flows.

## 5. REFERENCES

[1] G. Aubert and P. Kornprobst, *Mathematical Problems in Image Processing*, Springer, 2002.

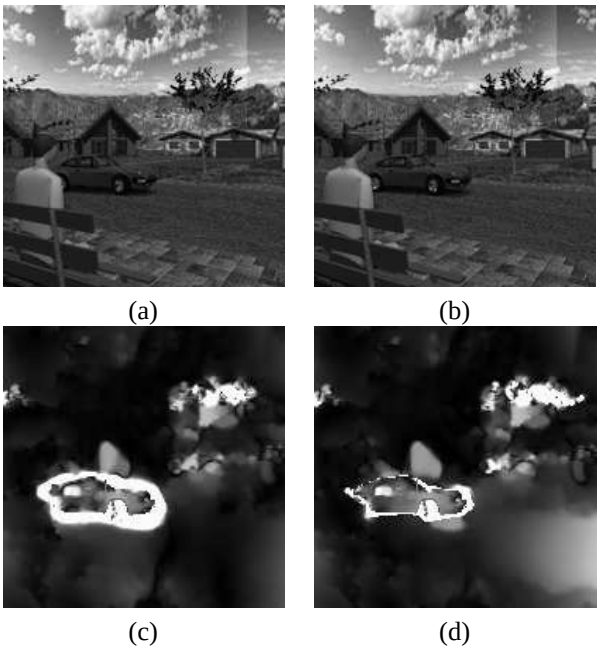

(a) (b) (c) (d)

**Fig. 2**. (a) Frame 10 of the *Street with car* sequence. (b) Frame 11. (c) Angular error with Brox *et al*'s 2D method (black: no error). (d) Angular error in our results.

| Technique | AAE | STD |
|---|---|---|
| Horn-Schunck [15] | 14.2° | |
| Proesmans *et al* [15] | 7.5° | |
| Brox *et al* (2D) | 3.03° | 10.18° |
| **Our method** | **2.82°** | **9.52°** |

**Table 2**. Comparison between several dense optical flow algorithms on the *Street with car* sequence. The numbers for the two first methods were derived from a graph in [15].

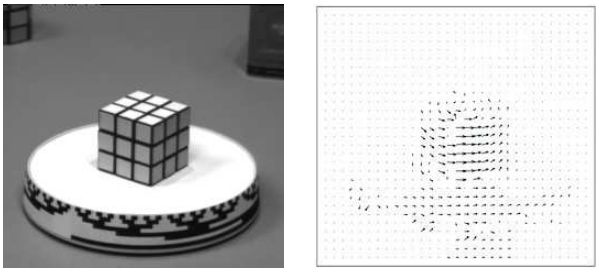

(a) (b)

**Fig. 3**. (a) Frame 19 of the *Rubic cube* sequence. (b) Computed flow field for the sequence.


[2] J.L. Barron, D.J. Fleet and S.S. Beauchemin, "Performance of Optical Flow Techniques," *International Journal of Computer Vision*, Vol. 12, pp. 43-77, 1994.

[3] B. Horn and B. Schunck, "Determining optical flow," *Artificial Intelligence*, Vol. 17, pp. 185-203, 1981.

[4] B. Lucas and T. Kanade, "An Iterative Image Registration Technique with Application to Stereo Vision," *Proc. DARPA Image Understanding Workshop*, pp. 121-130, 1981.

[5] D.J. Fleet and A.D. Jepson, "Computation of Component Image Velocity from Local Phase Information," *Int. J. Computer Vision*, Vol. 5, pp. 77-104, 1990.

[6] M.J. Black and D.J. Fleet, "Probabilistic Detection and Tracking of Motion Boundaries," *Int. J. Computer Vision*, Vol. 38, pp. 231-245, 2000.

[7] T. Brox, A. Bruhn, N. Papenberg, and J. Weickert, "High Accuracy Optical Flow Estimation Based on a Theory for Warping," *Proc. 8th European Conf. Computer Vision*, Vol. 4, pp. 25-36, 2004.

[8] P. Anandan, "A Computational Framework and an Algorithm for the Measurement of Visual Motion," *Int. J. Computer Vision*, Vol. 2, pp. 283-310, 1989.

[9] M.J. Black and P. Anandan, "The Robust Estimation of Multiple Motions: Parametric and Piecewise Smooth Flow Fields," *Computer Vision and Image Understanding*, Vol. 63, pp. 75-104, 1996.

[10] E. Mémin and P. Pérez, "A Multigrid Approach for Hierarchical Motion Estimation," *Proc. 6th Int. Conf. Computer Vision*, pp. 933-938, 1998.

[11] D. Mumford and J. Shah, "Optimal Approximation by Piecewise Smooth Functions and Associated Variational Problems," *Comm. Pure and Applied Mathematics* Vol. 42, pp. 577-685, 1989.

[12] L. Ambrosio and V.M. Tortorelli, "Approximation of Functionals Depending on Jumps by Elliptic Functionals via Γ-Convergence," *Comm. Pure and Applied Mathematics* Vol. 43, pp. 999-1036, 1990.

[13] L.A. Vese and T.F. Chan, "A Multiphase Level Set Framework for Image Segmentation Using the Mumford and Shah Model," *Int. J. Computer Vision*, Vol. 50, pp. 271-293, 2002.

[14] S. Osher and J.A. Sethian, "Fronts Propagating with Curvature Dependent Speed: Algorithms based on Hamilton-Jacobi Formulation," *J. Computational Physics*, Vol. 79, pp. 12-49, 1988.

[15] B. Galvin, B. McCane, K. Novins, D. Mason and S. Mills, "Recovering Motion Fields: An Evaluation of Eight Optical Flow Algorithms," *Proc. British Machine Vision Conference*, 1998.